Mitochondrial Function Regulated by Mitoguardin-1/2 Is Crucial for Ovarian Endocrine Functions and Ovulation

Xiao-Man Liu,[1,2,3] Yin-Li Zhang,[1] Shu-Yan Ji,[1] Long-Wen Zhao,[1] Wei-Na Shang,[1] Dali Li,[4] Zijiang Chen,[2,3] Chao Tong,[1] and Heng-Yu Fan[1]

[1]Life Sciences Institute and Innovation Center for Cell Signaling Network, Zhejiang University, Hangzhou 310058, China; [2]Center for Reproductive Medicine, Shandong Provincial Hospital Affiliated to Shandong University, Jinan, Shandong 250021, China; [3]The Key Laboratory for Reproductive Endocrinology of the Ministry of Education, Jinan, Shandong 250001, China; and [4]Shanghai Key Laboratory of Regulatory Biology, Institute of Biomedical Sciences and School of Life Sciences, East China Normal University, Shanghai 200241, China

The balances of mitochondrial dynamic changes, mitochondrial morphology, and mitochondrial number are critical in cell metabolism. Once they are disturbed, disorders in these processes generally cause diseases or even death in animals. We performed large-scale genetic screenings in fruit flies and discovered the mitoguardin gene (*Miga*) that encodes for a mitochondrial outer membrane protein. To examine the physiological functions of its mammalian homologs *Miga1* and *Miga2*, we generated *Miga1* and *Miga2* single- and double-knockout mouse strains and found that the knockout mice were viable, but the females were subfertile. The ovarian phenotypes of these mice suggested that the MIGA1/2 proteins play an important role in ovulation and ovarian steroidogenesis. *In vivo* and *in vitro* analyses of *Miga1/2*-knockout granulosa cells showed severe defects in luteinization and steroidogenesis and disordered mitochondrial morphology and function in response to gonadotropins. This is a report of genes involved in mitochondrial fusion and morphology-regulating mitochondrial functions during ovulation and luteinization. These results suggest a mechanism of gonadotropin-regulated ovarian endocrine functions and provide clues for therapeutic treatments of infertile females. (*Endocrinology* 158: 3988–3999, 2017)

The production of steroid hormones by the ovary, which plays a key role in female phenotype maintenance, is critical for regular ovarian processes, including follicle growth, oocyte maturation, and ovulation (1). Normal mitochondrial function is essential for ovarian steroidogenesis (2). Cholesterol is the precursor for the biosynthesis of estrogen and progesterone. Once inside the cell, free cholesterol is transported to the mitochondria through a mechanism that involves sterol carrier proteins. The cytochrome P450 cholesterol side chain cleavage enzyme (encoded by *Cyp11a1*) complex converts cholesterol to pregnenolone, which is then converted to progesterone by 3β-hydroxysteroid dehydrogenase in the smooth endoplasmic reticulum (3). The transport of cholesterol from the cytoplasm to the inner mitochondrial membrane is the rate-limiting step in progesterone biosynthesis (4). The steroidogenic acute regulatory protein and peripheral-type benzodiazepine receptors are proposed to be involved in this transport (5). It is known that the mitochondria of functional corpora lutea (CLs) of pregnancy are highly complex, with elongated and elaborate morphology. That the corpus luteum must synthesize enormous amounts of

progesterone requires elevated levels of adenosine triphosphate (ATP) and the reduced form of NAD phosphate.

Mitochondrial dynamics describes the sustainable variations of mitochondrial morphology in cells. It is regulated mainly by fusion and fission, which are critical processes in the maintenance of mitochondrial functions and metabolic homeostasis (6, 7). Mitochondrial fragmentation describes a variation on morphology of mitochondria, resulting in a shorter length compared with the tubular morphology. Unbalanced mitochondrial fusion and fission result in mitochondrial fragmentation. When fragmented, mitochondria change from the long tubular form into a short and round form, with fewer cristae inside. Generally, mitochondrial fragmentation causes decreased respiratory activity and ATP production (8). In mammals, several proteins have been implicated in the regulation of the fusion and fission of mitochondria. Mitofusin-1 and -2 together with the optic atrophy 1 protein are necessary for mitochondrial fusion, and the dynamin-related protein 1 is indispensable for fission (9–11). Each cell can contain several hundred copies of mitochondrial DNA (mtDNA) (10^3 to 10^4 copies per cell) depending on the energy demand of the tissue and differentiation stage of the cell. Previous reports have suggested that mitochondrial functions play important roles in both oocyte meiosis and embryo development (12). Mitochondrial dysfunction has been found in oocytes of people with obesity, diabetes, and insulin resistance (13, 14). To date, it remains unclear how mitochondrial fusion and fission regulate ovarian steroidogenesis and ovulation.

Recently, we identified a mitochondrial protein called mitoguardin (MIGA) in *Drosophila*. MIGA has two homologs, *Miga1* and *Miga2,* in vertebrates (15). MIGA protein is nuclear encoded and located on the outer membrane of the mitochondria. MIGA promotes mitochondrial fusion by interacting with the mitochondrial outer membrane protein mitochondrial phospholipase D (15).

To study the physiological function of the *Miga1/2* genes in mammals, we generated *Miga1* and *Miga2* single- and double-knockout mouse strains and found that the knockout females were subfertile. The ovarian phenotypes of these mice suggested that MIGA1/2 might play important roles in ovulation and ovarian steroidogenesis. *In vivo* and *in vitro* analyses of the *Miga1/2* knockout granulosa cells (GCs) revealed that they had severe defects in luteinization and steroidogenesis and disordered mitochondrial morphology and function in response to gonadotropins. This is a report of genes that are involved in mitochondrial fusion and morphology and regulate mitochondrial functions in the process of ovulation and luteinization.

Materials and Methods

Mice

The design of transcription activatorlike effector nuclease construction and generation of $Miga1^{-/-}$ (*Fam73a*) knockout mice was described previously (16). The potential targeted F0 animals were identified by T7 endonuclease digestion and sequencing. The heterozygous *Miga2*-knockout-first mice (strain ID: $Fam73b^{tm1a(KOMP)Wtsi}$) were originally obtained from the University of California, Davis Knockout Mouse Project Repository. Male and female heterozygous *Miga2*-knockout-first mice ($Miga2^{+/-}$) were mated to each other to produce control wild-type (WT) and homozygous knockout mice ($Miga2^{-/-}$). All mice were handled with care, and their handling was approved by the Animal Research Committee guidelines of Zhejiang University.

GC culture

GCs were harvested from pregnant mare serum gonadotropin (PMSG)–primed (24 hours), 23-day-old mice as described previously (17). Briefly, undifferentiated GCs were released from antral follicles by puncturing with a 26.5-gauge needle. Cells were cultured at a density of 1×10^6 cells in Dulbecco's modified Eagle medium (Invitrogen, Carlsbad, CA) containing 5% fetal bovine serum (Invitrogen), 100 U/mL penicillin, and 100 µg/mL streptomycin in 24-well culture dishes. To induce the expression of luteinizing hormone (LH) target genes and luteinization *in vitro,* GCs were treated with forskolin (FSK; 10 µM) and phorbol 12-myristate 13-acetate (PMA; 20 nM) for 2 to 24 hours.

Terminal deoxynucleotidyl transferase-mediated nick-end labeling assay

Analysis of apoptosis in WT and mutant mouse ovaries was carried out by terminal deoxynucleotidyl transferase-mediated nick-end labeling (TUNEL) assay with the ApopTag Plus *in situ* apoptosis detection kit (Chemicon International, Temecula, CA) according to the manufacturer's instructions.

Immunofluorescence

Ovaries were fixed in 4% paraformaldehyde, embedded in optimal cutting temperature compound (Sakura Finetek USA Inc., Torrance, CA), and stored at −70°C before the preparation of 7-µM sections. Sections were sequentially probed with primary antibodies, as indicated in the text, and secondary Alexa Fluor 594- or 488-conjugated goat anti-rabbit immunoglobulin G antibodies (Molecular Probes, Eugene, OR). Slides were mounted with VectaShield with 4′,6-diamidino-2-phenylindole (Vector Laboratories, Burlingame, CA).

For cultured GCs, cells were fixed with 4% paraformaldehyde for 20 minutes, permeabilized with 0.1% Triton X-100 for 10 minutes, and blocked with 5% bovine serum albumin for 30 minutes. The cells were then immunostained with primary antibodies against indicated antibodies for 1 hour, followed by washing and fluorescent dye–conjugated secondary antibody staining for 1 hour. Then the cells were mounted with VectaShield (Vector Laboratories), followed by microscopy.

All mounted samples were examined and imaged on a confocal microscope LSM710 (Carl Zeiss, Jena, Germany) outfitted with Plan-Apochromat ×40 or ×63 oil immersion

objective lenses (Carl Zeiss). Data were collected *via* Carl Zeiss software ZEN 2010 and processed in Image J and Photoshop CS (Adobe, San Jose, CA).

Histology and immunohistochemistry

Ovaries were collected and fixed in 4% paraformaldehyde, embedded in paraffin, and processed by routine procedures. Immunohistochemistry was done with VectaStain Elite avidin–biotin complex method kits (Vector Laboratories) as directed by the manufacturer. Sections were probed with primary antibodies against cleaved caspase-3 (Cell Signaling, CA) and cytochrome P450 family 11 subfamily A member 1 (CYP11A1) (Proteintech; catalog no. 13363-1-AP), and staining was done with the 3,3V-diaminobenzidine peroxidase substrate kit (Vector Laboratories) as directed. Sections were counterstained with hematoxylin, dehydrated, and mounted.

Transmission electron microscopy

Ovaries were washed in phosphate-buffered saline (PBS) and fixed in 2.5% glutaraldehyde, washed in PBS, and postfixed in 1% osmic acid for 1 to 2 hours. Then the samples were dehydrated and embedded in EMbed 812 (Electron Microscopy Sciences, Hatfield, PA) resin. Embedded samples were cut into 60-nm ultrathin sections. Sections were counterstained with uranyl acetate and lead citrate. All the samples were observed with a Hitachi HT7700 electron microscope (Hitachi Limited, Tokyo, Japan).

Mitochondrial membrane potential quantification

GCs were stained with JC-1 solution (5 μM in Dulbecco's modified Eagle medium; Invitrogen, Carlsbad, CA) for 30 minutes at 37°C. After cells were washed with PBS, they were mounted and observed with a confocal laser scanning microscope. The mitochondrial membrane potential was quantified by the ratio of the intensity of red fluorescence to green fluorescence. Flow cytometry was also performed to quantify the mitochondrial membrane potentials in cells. GCs were suspended by digesting with trypsin, washed, and stained with JC-1 for 30 minutes at 37°C. Then the GCs were washed and analyzed by flow cytometry (Beckmann).

Quantification for mtDNA copy number

GCs were lysed in 200 μL lysis buffer [50 mM Tris-HCl (pH 8.0), 1 mM EDTA, 0.5% Tween-20, 100 mg/mL protease K] and incubated at 55°C for 2 hours, then 95°C for 10 minutes, and the samples were directly used in real-time polymerase chain reaction primed by mtDNA specific primers (forward, TACCTCACCATCTCTTGCTA; reverse, CCACATAGACGAGTTGAT-TC). The value of the mtDNA was standardized by the value of the beta-globin.

Luminescence testing for ATP quantification

The ATP content of GCs was determined with the ATP Testing Assay Kit (Beyotime) according to the manufacturer's instructions. Briefly, 50 oocytes were lysed in ATP lysis buffer (from the kit) and centrifuged at 12,000*g* for 10 minutes. Supernatants were mixed with testing buffer, and ATP concentrations were measured on a luminescence detector.

Western blot analyses

Cell extracts containing 30 μg proteins were resolved by sodium dodecyl sulfate polyacrylamide gel electrophoresis and transferred to polyvinylidene fluoride membranes (Millipore Corp., Bedford, MA). After probing with primary antibodies, the membranes were incubated with horseradish peroxidase–linked anti-rabbit antibodies (Cell Signaling Technologies, Danvers, MA) and washed, and the bound antibodies were visualized with enhanced chemiluminescence substrate (Thermo Fisher Scientific, Waltham, MA).

RNA isolation and RT-PCR

For verification of the microarray analyses, total RNA was isolated from GCs of ≥ 3 mice. Reverse transcription was done with a SuperScript One-Step RT-PCR system with a Platinum Taq kit (Invitrogen). The reverse transcription polymerase chain reaction (RT-PCR) was performed with a 7500 Real-Time PCR System (Applied Biosystems, Foster City, CA). Relative messenger RNA (mRNA) levels were calculated by normalizing to the levels of endogenous β-actin mRNA (used as an internal control) in Microsoft Excel. For each indicated gene, the relative transcript level of the control sample was set at 1. The relative transcript levels of other samples were compared with the control. For each experiment, quantitative PCR reactions were done in triplicate.

Statistical analyses

The data for RT-PCR assays, breeding experiments, hormone levels, and superovulation tests are represented as means ± standard deviations. Data were analyzed in GraphPad Prism Programs (GraphPad Inc., San Diego, CA) to determine significance (analysis of variance or *t* test). Values were considered significantly different if $P \leq 0.05$ or $P \leq 0.01$.

Results

Miga1/2$^{-/-}$ female mice have reduced ovary size and fertility

Generation of *Miga1* and *Miga2* knockout mice was reported previously (15, 16). The *Miga1/2*$^{-/-}$ female mice exhibited reduced body size and weight compared with those of WT mice [Fig. 1(a)–1(c)]. The ovaries of *Miga1/2*$^{-/-}$ mice were smaller than those of WT mice from the pubertal (4-week-old) to late adult (1-year-old) stages [Fig. 1(d)]. *Miga1*$^{-/-}$, *Miga2*$^{-/-}$, and *Miga1/2*$^{-/-}$ males showed normal fertility, whereas the females were subfertile [Fig. 1(e)]. In a superovulation assay, WT mice generally ovulated at an average number of 46.6 oocytes per mouse, whereas *Miga1*$^{-/-}$, *Miga2*$^{-/-}$, and *Miga1/2*$^{-/-}$ mice ovulated at an average number of 21.5, 19.6, and 17.9 oocytes per mouse, respectively [Fig. 1(f)]. After superovulation, the ovaries of *Miga1*$^{-/-}$, *Miga2*$^{-/-}$, and *Miga1/2*$^{-/-}$ mice were smaller than those of WT mice [Fig. 1(g)]. Large CLs were formed in gonadotropin-treated WT ovaries but not in *Miga1/2*$^{-/-}$ ovaries [Fig. 1(g)]. Therefore, these mice had a reduced response to gonadotropins.
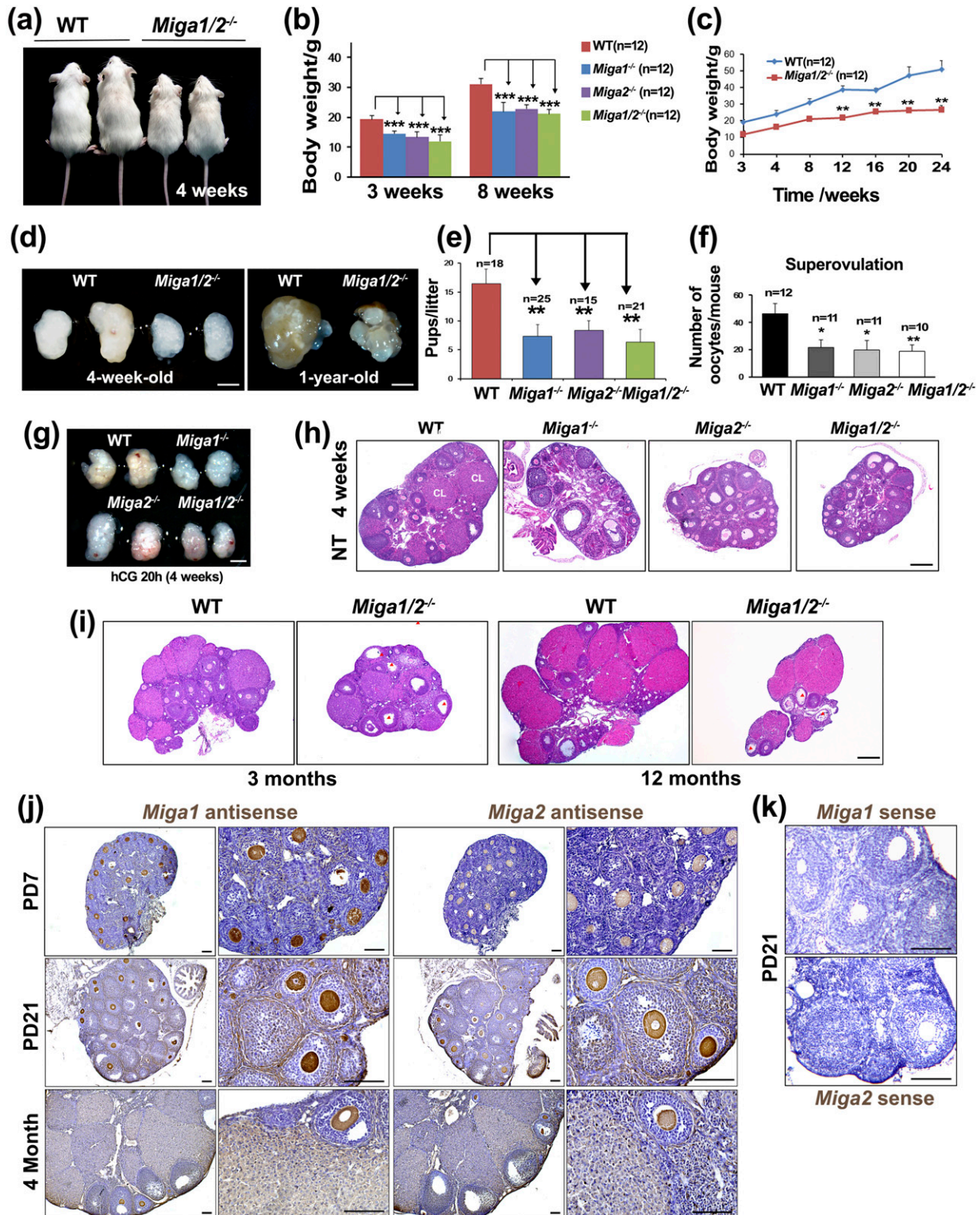
Figure 1. $Miga1/2^{-/-}$ mice exhibited reduced ovary size and body size. (a) $Miga1/2^{-/-}$ female mice had smaller body sizes compared with the control mice. (b) The body weights of mice of the indicated genotypes 3 to 8 weeks after birth. (c) Growth curves of the WT and $Miga1/2^{-/-}$ female mice from 3 to 24 weeks. (d) Ovaries from 4-week-old and 1-year-old WT and $Miga1/2^{-/-}$ mice. Scale bar = 1 mm. (e) Average pup numbers per litter of the indicated mouse strains. The total numbers (n) of mated females are indicated. (f) Average numbers of oocytes ovulated by mice of the indicated genotypes. The total numbers (n) of superovulated females are indicated. (g) Ovaries from superovulated WT and $Miga1/2^{-/-}$ mice. Scale bar = 1 mm. (h, i) Hematoxylin and eosin staining of the ovarian sections of 4-week-old, 3-month-old, and 12-month-old mice with the indicated genotypes. Scale bar = 250 μm. (j) *In situ* hybridization results showing the expression of *Miga1* and *Miga2* mRNA in mouse ovaries. Scale bar = 100 μm. (k) *In situ* hybridization with *Miga1*-sense and *Miga2*-sense probes on postnatal day (PD) 21 mouse ovaries as negative controls. Scale bar = 100 μm. *$P < 0.05$, **$P < 0.01$, and ***$P < 0.001$ were calculated by two-tailed Student t tests.

When we examined the follicles in the ovaries of the 4-week-old mice without hormone treatment, CLs were formed in the ovaries of the WT mice but not in the ovaries of the $Miga1^{-/-}$, $Miga2^{-/-}$, and $Miga1/2^{-/-}$ mice [Fig. 1(h)]. The ovaries of adult $Miga$ knockout mice (3 to 12 months old) contained fewer CLs and more atretic follicles than the WT controls, which suggested that $Miga1/2$-depleted GCs have defects of luteinization [Fig. 1(i)].

Because no antibodies were available to detect the endogenous MIGA1 and 2 proteins of mouse origin, we examined the expression pattern of $Miga1/2$ mRNA in mouse ovaries with *in situ* hybridization [Fig. 1(j) and 1(k)]. At postnatal day (PD) 7, both $Miga1$ and $Miga2$ were expressed in oocytes but not in ovarian somatic cells. At PD21, $Miga1/2$ expression was also detected in both GCs and theca cells. In the ovaries of adult females (4 months old), $Miga1$ and $Miga2$ were expressed in luteal cells and ovarian stroma cells [Fig. 1(j)].

Miga1 and Miga2 knockouts led to follicle atresia

To determine whether the $Miga1/2^{-/-}$ GCs were apoptotic, we performed TUNEL assays. A significant number of GCs were apoptotic in the follicles of the $Miga1^{-/-}$, $Miga2^{-/-}$, and $Miga1/2^{-/-}$ mice [Fig. 2(a) and 2(b)]. We verified these results with immunohistochemistry for cleaved caspase-3, which is an apoptotic cell marker [Fig. 2(a) and 2(c)].

We observed the ultrastructure of the $Miga1/2$-depleted GCs with transmission electron microscopy. In these cells, the chromatin was pycnotic. Their mitochondria were fragmented and had a round, short morphology. However, most mitochondria in the WT GCs had tubular or dumbbell shapes [Fig. 2(d) and 2(e)]. Condensed chromatin was also observed in the nuclei of $Miga1/2$-depleted GCs [Fig. 2(d), arrows], which indicated that these GCs were apoptotic. This finding was consistent with the results of the TUNEL staining [Fig. 2(a)]. FSK and PMA mimicked gonadotropin stimulation and induced the expression of follicle-stimulating hormone (FSH)/LH target genes in cultured GCs. As shown in Fig. 2(f), FSK/PMA increased the expression of the FSH target genes $Cyp19a1$ and $Fshr$, which are essential for maintaining follicle survival and growth. However, the expression of these genes was compromised in the GCs of $Miga1/2^{-/-}$ mice [Fig. 2(f)].
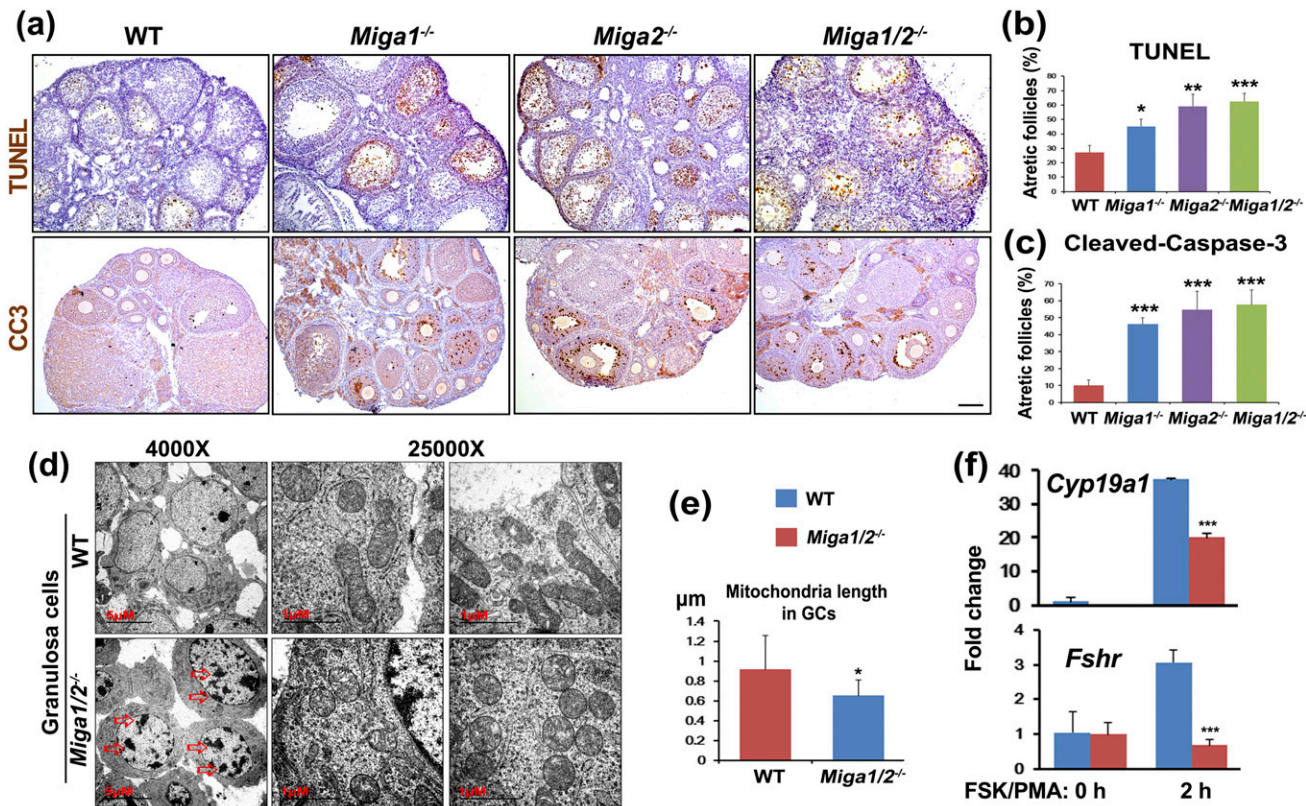
Figure 2. GC apoptosis in the ovaries of $Miga1/2^{-/-}$ mice. (a–c) TUNEL assay and immunohistochemistry of cleaved caspase-3 (CC3) showing GC apoptosis in the ovaries of WT and $Miga1/2^{-/-}$ mice (3~4 weeks old). Scale bar = 100 μm. (d, e) Transmission electron microscopy results showing condensed chromatin and shortened mitochondria in the GCs of $Miga1/2^{-/-}$ mice (3~4 weeks old). Scale bar = 5 μm or 1 μm as indicated. (f) Quantitative RT-PCR for $Cyp19a1$ and $Fshr$ in cultured GCs before and after FSK and PMA treatment. $*P < 0.05$, $**P < 0.01$, and $***P < 0.001$ were calculated by two-tailed Student t tests.

Ovulation and luteinization were compromised in *Miga1/2*$^{-/-}$ ovaries

As shown in the superovulation assay, the number of ovulated oocytes was greatly reduced in *Miga1/2*$^{-/-}$ mice, and we observed arrested oocytes in the follicles 16 hours after human chorionic gonadotropin (hCG) treatment. At this time, the WT mice had ovulated, and well-expanded cumulus–oocyte complexes were found in the oviducts [Fig. 3(a)]. However, multiple unruptured large antral follicles were present in the ovaries of *Miga1/2*$^{-/-}$ mice. In these follicles, cumulus cells had already dissociated from the oocytes [Fig. 3(a)]. After exposure to hCG for 48 to 72 hours, results of quantitative RT-PCR analyses showed that *Miga1* and *Miga2* mRNAs were expressed in isolated luteal cells, and their levels were higher than those in PMSG-primed GCs [Fig. 3(b)]. Many fewer CLs were formed in the *Miga1/2*$^{-/-}$ ovaries, and unovulated oocytes were trapped in these CLs [Fig. 3(c)]. In addition, these hCG-treated *Miga1/2*$^{-/-}$ mice had significantly lower serum progesterone levels compared with WT mice [Fig. 3(d)].

FSK/PMA triggered progesterone secretion [Fig. 3(d)] and induced the expression of luteinization marker genes (*Lhcgr, Cyp11a1, Sfrp4,* and *Star*) in GCs isolated from WT mice [Fig. 3(e)]. However, the progesterone biosynthesis, as well as expression of luteinization-related genes, was significantly reduced in GCs from *Miga1/2*$^{-/-}$ mice [Fig. 3(d) and 3(e)]. At the submicroscopic level, the mitochondria of GCs underwent dramatic structural transformations during luteinization when they changed from a narrow shape into a round shape, and the mitochondrial cristae were extended and broadened to form a network for increased steroidogenesis [Fig. 3(f)]. Usually, mitochondria in metabolically active cells (including steroidogenic cells) have more tubular cristae. The structure of tubular cristae increased the total surface of mitochondrial inner membrane and strengthened the mitochondrial activity (18). However, these ultrastructural mitochondrial changes were compromised in the luteal cells of *Miga1/2*$^{-/-}$ mice [Fig. 3(f)].

CYP11A1, the key enzyme of progesterone biosynthesis, was expressed in luteal cells after LH/hCG stimulation and localized to mitochondria. The immunohistochemistry results showed that the CLs of *Miga1/2*$^{-/-}$ mice had lower levels of CYP11A1 expression compared with the WT mice 48 hours after hCG treatment [Fig. 3(g)]. When cultured GCs were induced to luteinize *in vitro,* a moderate rate of cell apoptosis that was characterized by caspase-3 activation was detected by Western blot [Fig. 3(h)] and immunofluorescence [Fig. 3(i)]. However, stronger apoptosis signals were detected in *Miga1/2*$^{-/-}$ GCs [Fig. 3(h) and 3(i)], which suggested that these GCs did not luteinize properly.

Expression of LH target genes was inhibited in *Miga1/2*$^{-/-}$ GCs

We investigated whether *Miga1/2*$^{-/-}$ GCs responded normally to gonadotropins. The follicles in *Miga1/2*$^{-/-}$ ovaries responded poorly to PMSG and hCG, which showed that fewer follicles were activated to grow into mature antral follicles [Fig. 4(a) and 4(b)]. Generally, the germinal vesicle breakdown of oocytes occurred about 4 hours after hCG injections in the *Miga1/2*$^{-/-}$ oocytes *in vivo* [Fig. 4(b)]. At that moment, the cumulus expansion–related LH target genes were activated in WT follicles. The proteins encoded by *Ptx3* and *Ptgs2* accumulated in the preovulatory follicles of WT ovaries after hCG treatment [Fig. 4(c)]. However, their levels were low in GCs of the *Miga1/2*$^{-/-}$ mice [Fig. 4(c)]. As a result, the cumulus–oocyte complex (circled in red) did not expand in the ovaries of *Miga1/2*$^{-/-}$ mice 8 hours after hCG injection [Fig. 4(d)]. Additionally, in cultured GCs that were isolated from *Miga1/2*$^{-/-}$ mice, the expression of LH target genes, such as *Ereg, Btc, Ptx3, Ptgs2, Tnfaip6,* and *Has2,* was compromised after FSK/PMA treatment, which mimicked LH stimulation *in vitro* [Fig. 4(e)]. Because *Miga1/2* are also expressed in mouse oocytes and important for oocyte functions, we examined the expression of oocyte genes *Gdf9* and *Bmp15,* which encode factors secreted by oocytes that enable cumulus expansion. Quantitative RT-PCR results showed that *Gdf9* and *Bmp15* mRNA expression levels in oocytes of *Miga1/2*$^{-/-}$ mice were significantly lower than those in WT oocytes [Fig. 4(f)]. This observation suggests that compromised oocyte function may also contribute to the ovulation defects of *Miga1/2*$^{-/-}$ mice.

Miga1/2$^{-/-}$ GCs had impaired functions and morphology in mitochondria

We further assessed the mitochondrial characteristics of the GCs of *Miga1/2*$^{-/-}$ mice. GCs isolated from WT mice had a tubular and reticulated mitochondrial network in the cytoplasm. However, the mitochondria were fragmented after 24 hours of FSK/PMA treatment. The mitochondria in *Miga1/2*$^{-/-}$ GCs were mostly fragmented, even before FSK/PMA treatment [Fig. 5(a)]. This finding is consistent with our previous observations in cultured embryonic fibroblasts isolated from *Miga1/2*$^{-/-}$ mice (15). The mitochondrial membrane potential increased in WT GCs after treatment with FSK/PMA for 2 hours [Fig. 5(b)]. However, the mitochondrial membrane potential levels in *Miga1/2*$^{-/-}$ GCs were lower than those in WT GCs after FSK/PMA treatment [Fig. 5(b)]. In addition, the ATP contents and mtDNA copy numbers in *Miga1/2*$^{-/-}$ GCs were reduced after FSK/PMA treatment [Fig. 5(c) and 5(d)]. The reduction of mtDNA copy number is an indication of mitochondrial genome instability and a hallmark of defective mitochondria. Taken together, these
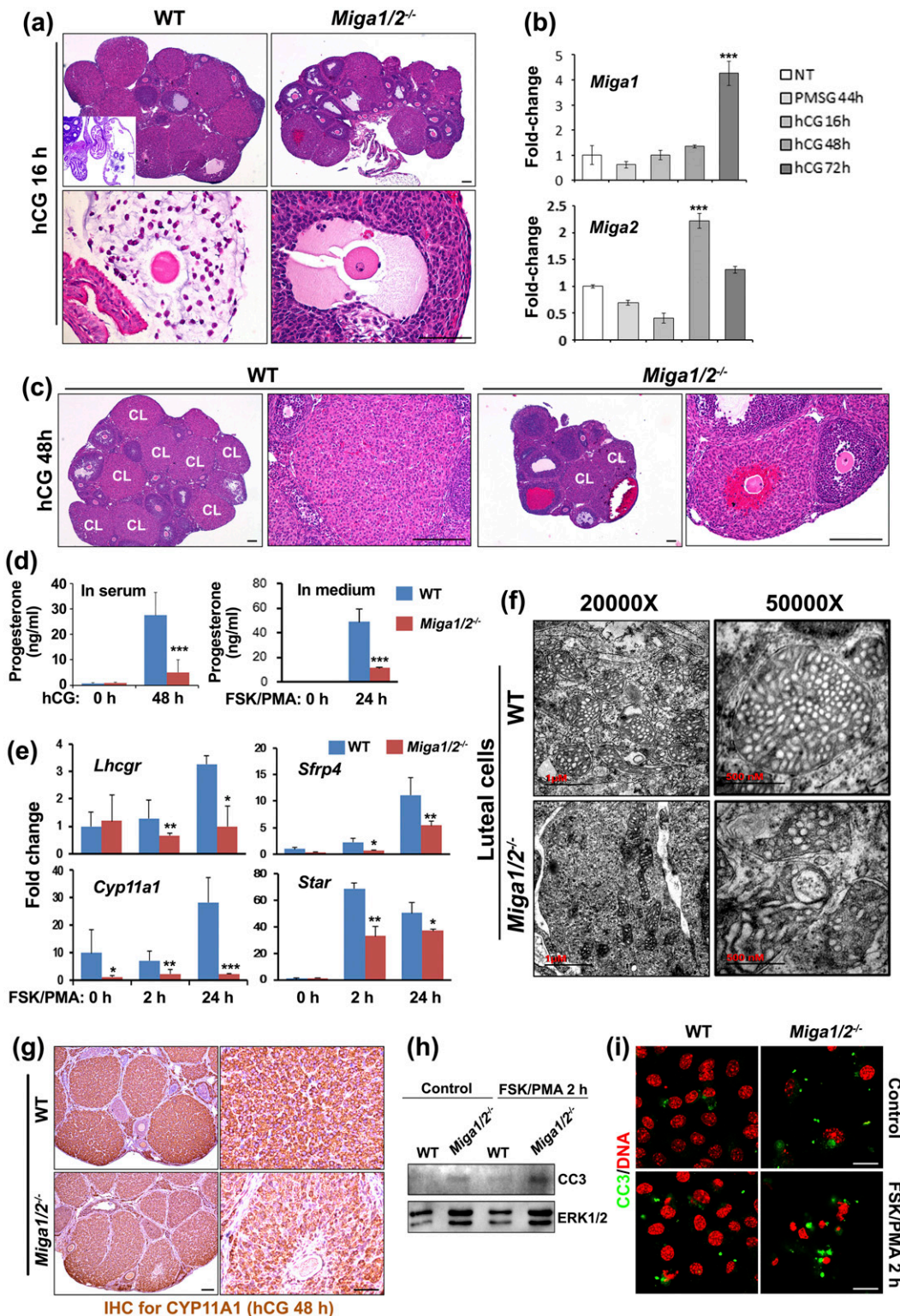
Figure 3. Ovulation and luteinization were blocked in the ovaries of *Miga1/2*$^{-/-}$ mice. (a) The oocytes were trapped in the follicles of the mutant mice with the indicated genotypes 16 hours after human chorionic gonadotropin (hCG) injections. Scale bar = 100 μm. (b) Quantitative RT-PCR results showing expression levels of *Miga1* and *Miga2* mRNAs in GCs and luteal cells isolated from 23-day-old mice treated with PMSG and hCG with indicated time intervals. NT, not treated with gonadotropin. (c) Ovarian histology of WT and *Miga1/2*$^{-/-}$ mice 48 hours after hCG injections. Scale bar = 250 μm. (d) Progesterone concentrations in mouse serum and GC culture medium after FSK/PMA treatment. (e) Quantitative RT-PCR for LH target luteal cell marker genes (*Lhcgr, Sfrp4, Cyp11a1,* and *Star*) in cultured GCs treated with FSK/PMA. (f) Transmission electron microscopy results showing the ultrastructure of mitochondria in luteal cells of WT and *Miga1/2*$^{-/-}$ mice. The luteal cells were collected from 3-week-old mice that were treated with PMSG 44 hours/hCG 48 hours. CLs were dissected under a stereoscope and then processed for transmission electron microscopy. Scale bar = 1 μm or 500 nm as indicated. (g) Immunohistochemistry for CYP11A1 expression in ovaries 48 hours after hCG injections. Scale bar = 100 μm. (h–i) Western blot (h) and immunofluorescence (i) for cleaved caspase-3 (CC3) in

results indicate that $Miga1/2^{-/-}$ GCs had impaired mitochondrial function and morphology.

The mitochondrion-targeted chemicals carbonyl cyanide *m*-chlorophenylhydrazone and mitochondrial division inhibitor-1 inhibit GC responses to ovulation signals

Because MIGA1/2 are mitochondrial proteins that regulate mitochondrial morphology and ATP production in mouse embryonic fibroblasts (MEFs) and oocytes, we applied the mitochondrion-targeted drugs carbonyl cyanide *m*-chlorophenylhydrazone (CCCP) and mitochondrial division inhibitor-1 (Mdivi-1) to cultured mouse GCs to observe whether they had the same effects that the *Miga1/2* knockout did. After CCCP or Mdivi-1 treatment, the GCs became round in shape [Fig. 5(e)]. FSK/PMA stimulation induced the expression of LH target genes (*Areg, Ereg,* and *Btc*) that encode for epidermal growth factor–like factors that are needed for cumulus expansion and ovulation in GCs. However, this effect was inhibited by CCCP or Mdivi-1 treatment [Fig. 5(f)]. Additionally, CCCP or Mdivi-1 treatment reduced FSK/PMA-triggered progesterone synthesis by GCs [Fig. 5(g)]. These results suggested that, similar to the *Miga1/2* gene knockouts, CCCP and Mdivi-1 caused GC functional defects by affecting mitochondrial function.

It appears that the small molecule disruptors of mitochondrial functions inhibit GC responses to ovulation signals more prominently than *Miga1/2* knockout. We evaluated the mRNA expression levels for several known genes (*Mfn1, Mitopld, Opa1*), which are involved in the regulation of mitochondrial fusion and fission, in GCs of PMSG-primed WT and $Miga1/2^{-/-}$ mice. The expression of these genes was significantly greater in *Miga1/2* knockout mice [Fig. 5(h)], suggesting that the increased expression of these mitochondrial genes might compensate the loss of *Miga1/2 in vivo.*

Discussion

Our study reports the mitochondrial genes *Miga1/2* regulating mitochondrial dynamics in mouse GCs. MIGA1/2 are required for mitochondrial functions in both GCs and in oocytes, and their knockout led to a reduction of female fertility (19). Deletion of the genes impaired mitochondrial functions such as mitochondrial dynamics and ATP production in GCs, as in cultured human cell lines (15) and in oocytes (19). Mitochondrial dysfunction led to female subfertility, as shown by the

Miga1/2-knockout mice. Mitochondrial dynamics describes the sustainable variations of the mitochondrial morphology in cells. Mitochondrial dynamics includes mainly mitochondrial fusion and fission. We have reported that depletion of *Miga1/2* led to mitochondrial fragmentation through inhibition of fusion in MEFs (15). Because the cellular function of MIGA1/2 has already been clearly addressed, and *Miga1/2* knockout female mice were subfertile because of impaired ovarian function, we focused on the physiological influence of *Miga1/2* depletion in ovarian GCs in this study. Female fertility is related not only to oocyte quality but also to the response of the FSH/LH target genes in GCs that promote follicle growth, ovulation, and CL formation (20, 21). In *Miga1/2* knockout females, the impaired ovulation observed in superovulation experiments appears to be caused by defects of both follicle development and terminal differentiation of GCs. The GCs are a group of special somatic cells that can be transformed to luteal cells that produce mainly progesterone, estradiol, and other steroid hormones. Mitochondria are the location of the biosynthesis of cholesterol, steroids, and lipids, particularly on the inner membrane (22). Therefore, regulation of mitochondrial dynamics is essential for GC function. The disruption of mitochondrial dynamics and metabolism is more likely to disrupt the biogenesis of hormones produced in the GCs and thus lead to defects in female reproduction.

However, to date few studies have examined the effects of mitochondrial dynamic regulation on hormone production in GCs. Herein, we report that the mitochondrial proteins MIGA1/2 are necessary for luteinization and progesterone biogenesis. Progesterone plays a central role in female reproduction because it promotes cumulus–oocyte complex expansion (23, 24). In addition, it is critical for ovulation in response to the pituitary LH surge (25). MIGA1/2 might play a role in mediating the transfer of the proteins involved in progesterone biogenesis from cytoplasm into mitochondria. CYP11A1 is an important enzyme that is localized on the mitochondrial inner membrane (26). CYP11A1 catalyzes cholesterol to pregnenolone, which is the precursor of progesterone. Depletion of the outer membrane proteins MIGA1/2 not only impaired basic mitochondrial functions by disrupting the mitochondrial metabolism that produced ATP but also reduced the expression of steroidogenic enzymes, resulting in a reduction in progesterone levels.

Mitochondria form a dynamic network. The loss of mtDNA indicates an increase in mitochondrial genome instability or defective mtDNA replication (27). The loss

---

Figure 3. (Continued). cultured GCs isolated from WT and $Miga1/2^{-/-}$ mice before and after FSK/PMA treatment. Extracellular signal-regulated kinase (ERK) 1/2 was blotted as an internal loading control. Scale bar = 10 μm. *$P < 0.05$, **$P < 0.01$, and ***$P < 0.001$ were calculated by two-tailed Student *t* tests.
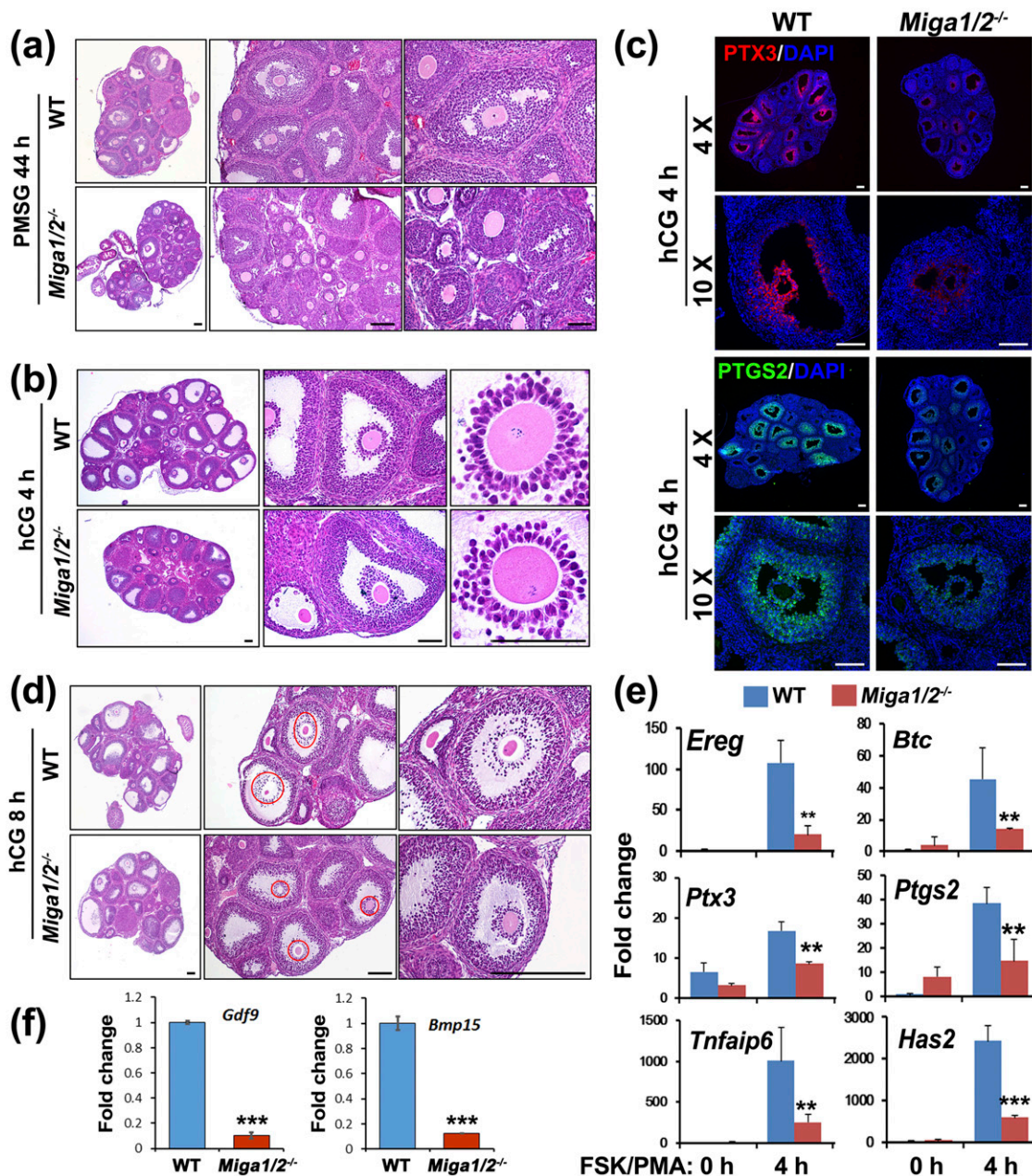
Figure 4. The expression of LH target genes was inhibited in $Miga1/2^{-/-}$ GCs. (a) Ovarian histology of the PMSG-primed (44 hours) WT and $Miga1/2^{-/-}$ mice. Scale bar = 100 μm. (b) Ovarian histology of WT and $Miga1/2^{-/-}$ mice 4 hours after hCG treatment. Scale bar = 100 μm. (c) Immunofluorescence of the cumulus–oocyte complex expansion-related proteins (PTX3 and PTGS2) in the ovaries of WT and $Miga1/2^{-/-}$ mice 4 hours after hCG treatment. Scale bar = 100 μm. (d) Ovarian histology of the WT and $Miga1/2^{-/-}$ mice 8 hours after hCG treatment. Representative expanding cumulus–oocyte complexes are circled in red. Scale bar = 100 μm. (e) Quantitative RT-PCR results for the LH target genes in GCs before and after FSK/PMA treatment. (f) Quantitative RT-PCR results for the oocyte genes (*Gdf9* and *Bmp15*) in oocytes isolated from 4-week-old WT and $Miga1/2^{-/-}$ mice. **$P < 0.01$ and ***$P < 0.001$ were calculated by two-tailed Student t tests. DAPI, 4′,6-diamidino-2-phenylindole.

of mtDNA here is more likely to be a functional loss because we did not observe obvious mitochondrial mass reduction by immunostaining of the mitochondria. In our study, we found that the reduction of mtDNA number in *Miga1/2* knockout cells was not associated with reduction of ATP synthesis. A possible explanation is that without stimulation, the mitochondria in cells do not need to reach full respiration capacity, and the remaining respiration capacity in *Miga1/2* knockout cells is

sufficient to produce ATP. FSK/PMA treatment boosts mitochondrial respiration to a high level in WT cells but cannot stimulate the defective mitochondria in *Miga1/2* knockout cells.

Once the biogenesis of progesterone and other related proteins is disordered on the inner membrane, it might damage the mitochondrial ultrastructure, which might be reflected in the short and round mitochondria with narrow cristae that were observed in MIGA1/2-depleted
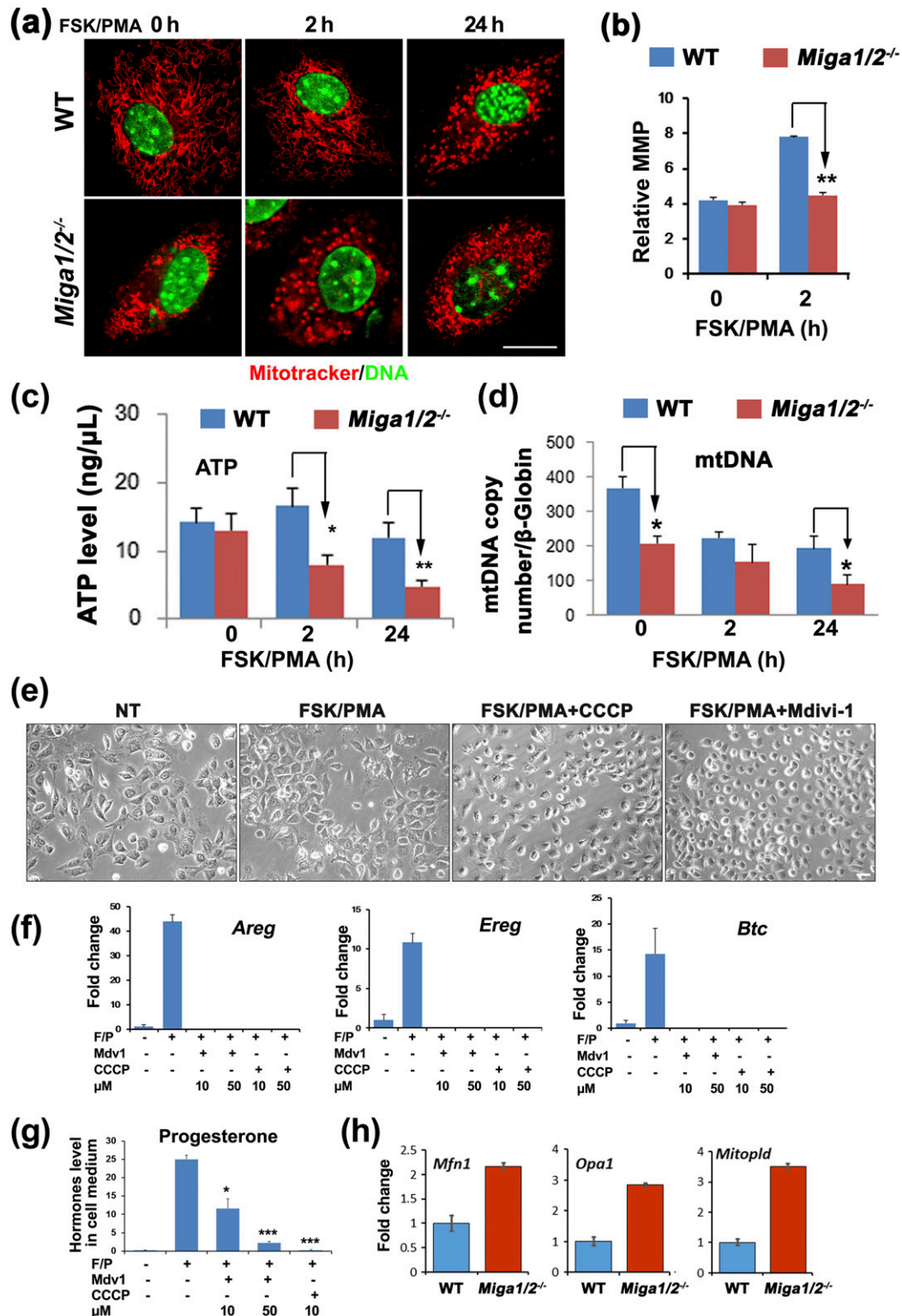
Figure 5. Variations of mitochondrial morphologies and mitochondrial activities after FSK/PMA treatment. (a) The mitochondrial morphologies varied after FSK/PMA treatments for different times in WT and *Miga1/2*[−/−] GCs. Scale bar = 5 μm. (b) Histograms of the mitochondrial membrane potentials (MMPs) assessed by flow cytometry. Variations in (c) ATP levels and (d) mtDNA copy numbers in WT and *Miga1/2*[−/−] GCs with or without FSK/PMA treatment. (e) Images of GCs treated with FSK/PMA with or without CCCP or mitochondrial division inhibitor-1 (Mdivi-1). Scale bar = 10 μm. (f) Quantitative RT-PCR for the epidermal growth factor–like factors in GCs treated with FSK/PMA (F/P) with or without CCCP or Mdivi-1 (Mdv1). (g) Progesterone levels in culture medium of cells treated with FSK/PMA with or without CCCP or Mdivi-1. (h) Quantitative RT-PCR for the indicated genes involved in the regulation of mitochondrial fusion and fission in GCs of PMSG-primed WT and *Miga1/2*[−/−] mice. *$P < 0.05$, **$P < 0.01$, and ***$P < 0.001$ were calculated by two-tailed Student t tests. NT, not treated.

Appendix.   Antibody Table

Peptide/ Protein Target	Antigen Sequence (If Known)	Name of Antibody	Manufacturer, Catalog No.	Species Raised in; Monoclonal or Polyclonal	Dilution Used	RRID
5A1E	Asp175	Cleaved caspase-3	Cell Signaling Technology, 9664	Rabbit; monoclonal	1:500	AB_2070042
N terminal	RMLLQATDDVLRGEL QRLREELGRLAESL ARPCAPGAPAEAR LTSALDEL	PTX3	Fitzgerald Industries International, 70R-5923	Rabbit; polyclonal	1:200	AB_10811543
K-20		PTGS2/COX2	Santa Cruz Biotechnology, sc-23984	Goat; polyclonal	1:200	AB_2066362

Abbreviation: RRID, Research Resource Identifier.

GCs. Mitochondrial fragmentation and leakage have been reported to be an important step in the induction of cell apoptosis (28), and MIGA1/2 deletion was found to induce mitochondrial fragmentation and cell apoptosis, especially in GCs around the oocytes.

The mitochondria-targeted compound CCCP uncoupled the mitochondrial membrane potential, disrupted the ATP metabolism process, induced mitochondrial fragmentation, and inhibited mitochondrial fusion, which are effects that are similar to the phenotype of *Miga1/2* deletion in MEFs. The phenotype in *Miga1/2*$^{-/-}$ GCs was similar to that of CCCP-treated GCs *in vitro,* which indicated that MIGA1/2 might regulate mitochondrial activities through the respiratory chain by regulating mitochondrial morphology remodeling. Furthermore, the lack of ATP might contribute to severe damage in the ultrastructure of the mitochondrial cristae.

Except for the defects in ovarian follicle development and ovulation, *Miga1/2* knockout females are generally normal and healthy. This observation suggests that MIGA1/2 are indispensable in ovary, but their functions can be compensated by other mitochondrial proteins in other organs. Results of *in situ* hybridization showed that *Miga1/2* mRNAs were expressed in both oocytes and ovarian somatic cells. We reported recently that MIGA1/2 were important for mitochondrial functions in oocytes (19). The quality and development potential of mouse oocytes decreased after *Miga1/2* knockout. When isolated and cultured *in vitro,* both oocytes and GCs showed abnormal mitochondrial distributions and morphology, as well as decreased ATP production. Therefore, the subfertility phenotypes observed in *Miga1/2* knockout females were probably caused by combined defects in both oocytes and GCs. Although the relationship between mitochondrial quality and oocyte quality has been widely recognized, the contributions of inherited mitochondrial defects in GCs to female reproductive disorders were not extensively addressed. Our analyses of ovarian function in *Miga1/2* knockout mice demonstrated the importance of

mitochondrial dynamics in female reproduction and steroidogenesis.

Acknowledgments

Correspondence and Reprint Requests: Heng-Yu Fan, PhD, Life Sciences Institute, Zhejiang University, 866 Yuhangtang Road, Hangzhou 310058, China. E-mail: hyfan@zju.edu.cn.

Disclosure Summary: The authors have nothing to disclose.

References

1. Liu Z, Rudd MD, Hernandez-Gonzalez I, Gonzalez-Robayna I, Fan HY, Zeleznik AJ, Richards JS. FSH and FOXO1 regulate genes in the sterol/steroid and lipid biosynthetic pathways in granulosa cells. *Mol Endocrinol.* 2009;**23**(5):649–661.

2. Chien Y, Rosal K, Chung BC. Function of CYP11A1 in the mitochondria. *Mol Cell Endocrinol.* 2017;**441**:55–61.

3. Miller WL, Auchus RJ. The molecular biology, biochemistry, and physiology of human steroidogenesis and its disorders. *Endocr Rev.* 2011;**32**(1):81–151.

4. Anuka E, Gal M, Stocco DM, Orly J. Expression and roles of steroidogenic acute regulatory (StAR) protein in "non-classical," extra-adrenal and extra-gonadal cells and tissues. *Mol Cell Endocrinol.* 2013;**371**(1–2):47–61.

5. Light A, Hammes SR. Membrane receptor cross talk in steroidogenesis: recent insights and clinical implications. *Steroids.* 2013;**78**(6):633–638.

6. Bach D, Naon D, Pich S, Soriano FX, Vega N, Rieusset J, Laville M, Guillet C, Boirie Y, Wallberg-Henriksson H, Manco M, Calvani M, Castagneto M, Palacín M, Mingrone G, Zierath JR, Vidal H, Zorzano A. Expression of Mfn2, the Charcot–Marie–Tooth neuropathy type 2A gene, in human skeletal muscle: effects of type 2 diabetes, obesity, weight loss, and the regulatory role of tumor necrosis factor alpha and interleukin-6. *Diabetes.* 2005;**54**(9):2685–2693.

7. Wang X, Su B, Lee HG, Li X, Perry G, Smith MA, Zhu X. Impaired balance of mitochondrial fission and fusion in Alzheimer's disease. *J Neurosci.* 2009;**29**(28):9090–9103.

8. del Campo A, Parra V, Vásquez-Trincado C, Gutiérrez T, Morales PE, López-Crisosto C, Bravo-Sagua R, Navarro-Marquez MF, Verdejo HE, Contreras-Ferrat A, Troncoso R, Chiong M, Lavandero S. Mitochondrial fragmentation impairs insulin-dependent glucose uptake by modulating Akt activity through mitochondrial Ca2+ uptake. *Am J Physiol Endocrinol Metab.* 2014; **306**(1):E1–E13.

9. Chen H, Detmer SA, Ewald AJ, Griffin EE, Fraser SE, Chan DC. Mitofusins Mfn1 and Mfn2 coordinately regulate mitochondrial fusion and are essential for embryonic development. *J Cell Biol.* 2003;**160**(2):189–200.

10. Cipolat S, Martins de Brito O, Dal Zilio B, Scorrano L. OPA1 requires mitofusin 1 to promote mitochondrial fusion. *Proc Natl Acad Sci USA.* 2004;**101**(45):15927–15932.

11. Frank S, Gaume B, Bergmann-Leitner ES, Leitner WW, Robert EG, Catez F, Smith CL, Youle RJ. The role of dynamin-related protein 1, a mediator of mitochondrial fission, in apoptosis. *Dev Cell.* 2001;**1**(4):515–525.

12. Van Blerkom J. Mitochondrial function in the human oocyte and embryo and their role in developmental competence. *Mitochondrion.* 2011;**11**(5):797–813.

13. Moran LJ, Pasquali R, Teede HJ, Hoeger KM, Norman RJ. Treatment of obesity in polycystic ovary syndrome: a position statement of the Androgen Excess and Polycystic Ovary Syndrome Society. *Fertil Steril.* 2009;**92**(6):1966–1982.

14. Ogbuji QC. Obesity and reproductive performance in women. *Afr J Reprod Health.* 2010;**14**(3):143–151.

15. Zhang Y, Liu X, Bai J, Tian X, Zhao X, Liu W, Duan X, Shang W, Fan HY, Tong C. Mitoguardin regulates mitochondrial fusion through MitoPLD and is required for neuronal homeostasis. *Mol Cell.* 2016;**61**(1):111–124.

16. Qiu Z, Liu M, Chen Z, Shao Y, Pan H, Wei G, Yu C, Zhang L, Li X, Wang P, Fan HY, Du B, Liu B, Liu M, Li D. High-efficiency and heritable gene targeting in mouse by transcription activator-like effector nucleases. *Nucleic Acids Res.* 2013;**41**(11):e120.

17. Fan HY, Shimada M, Liu Z, Cahill N, Noma N, Wu Y, Gossen J, Richards JS. Selective expression of KrasG12D in granulosa cells of the mouse ovary causes defects in follicle development and ovulation. *Development.* 2008;**135**(12):2127–2137.

18. Zick M, Rabl R, Reichert AS. Cristae formation-linking ultrastructure and function of mitochondria. *Biochim Biophys Acta.* 2009;**1793**(1):5–19.

19. Liu XM, Zhang YP, Ji SY, Li BT, Tian X, Li D, Tong C, Fan HY. Mitoguardin-1 and -2 promote maturation and the developmental potential of mouse oocytes by maintaining mitochondrial dynamics and functions. *Oncotarget.* 2016;**7**(2):1155–1167.

20. Fan HY, Liu Z, Johnson PF, Richards JS. CCAAT/enhancer-binding proteins (C/EBP)-α and -β are essential for ovulation, luteinization, and the expression of key target genes. *Mol Endocrinol.* 2011;**25**(2):253–268.

21. Fan HY, O'Connor A, Shitanaka M, Shimada M, Liu Z, Richards JS. Beta-catenin (CTNNB1) promotes preovulatory follicular development but represses LH-mediated ovulation and luteinization. *Mol Endocrinol.* 2010;**24**(8):1529–1542.

22. Dioguardi CC, Uslu B, Haynes M, Kurus M, Gul M, Miao DQ, De Santis L, Ferrari M, Bellone S, Santin A, Giulivi C, Hoffman G, Usdin K, Johnson J. Granulosa cell and oocyte mitochondrial abnormalities in a mouse model of fragile X primary ovarian insufficiency. *Mol Hum Reprod.* 2016;**22**(6):384–96.

23. Hammes SR, Levin ER. Minireview: recent advances in extranuclear steroid receptor actions. *Endocrinology.* 2011;**152**(12):4489–4495.

24. Jamnongjit M, Gill A, Hammes SR. Epidermal growth factor receptor signaling is required for normal ovarian steroidogenesis and oocyte maturation. *Proc Natl Acad Sci USA.* 2005;**102**(45): 16257–16262.

25. Robker RL, Russell DL, Espey LL, Lydon JP, O'Malley BW, Richards JS. Progesterone-regulated genes in the ovulation process: ADAMTS-1 and cathepsin L proteases. *Proc Natl Acad Sci USA.* 2000;**97**(9):4689–4694.

26. Clemens JW, Lala DS, Parker KL, Richards JS. Steroidogenic factor-1 binding and transcriptional activity of the cholesterol side-chain cleavage promoter in rat granulosa cells. *Endocrinology.* 1994;**134**(3):1499–1508.

27. Chen H, Vermulst M, Wang YE, Chomyn A, Prolla TA, McCaffery JM, Chan DC. Mitochondrial fusion is required for mtDNA stability in skeletal muscle and tolerance of mtDNA mutations. *Cell.* 2010;**141**(2):280–289.

28. Leboucher GP, Tsai YC, Yang M, Shaw KC, Zhou M, Veenstra TD, Glickman MH, Weissman AM. Stress-induced phosphorylation and proteasomal degradation of mitofusin 2 facilitates mitochondrial fragmentation and apoptosis. *Mol Cell.* 2012;**47**(4):547–557.